1 **Kelp Forest model development in the *Coupled Ocean-Atmosphere-Wave-***

2 ***Sediment-Transport model (COAWST V3.4)***

4 Matheus Fagundes[1]; Fiorenza Micheli[2,3]; Stephen G. Monismith[4]; Arnoldo Valle-Levinson[5]; C. Brock

5 Woodson[1]

6 [1] Department of Engineering, University of Georgia, Athens, GA, USA

7 [2] Ocean Department, Hopkins Marine Station, Stanford University, Pacific Grove, CA, USA

8 [3] Stanford Center for Ocean Solutions, Pacific Grove, CA, USA

9 [4] Monterey Bay Aquarium Research Institute, Moss Landing, CA, USA

10 [5] Civil and Coastal Engineering Department, University of Florida, Gainesville, FL, USA

12 Corresponding author:

13 Matheus Fagundes, mf99274@uga.edu

ABSTRACT

16 Kelp forests are essential ecosystems in coastal regions around the world. They have large

17 effects on flow structure, biogeochemical processes, and ecological dynamics. However,

18 studies have yet to simulate these ecosystems in either regional ocean or global climate models.

19 Here we describe and validate a model that simulates kelp forests in the water column for the

20 ocean component of the *Coupled Ocean-Atmosphere-Wave-Sediment-Transport model*

21 *(COAWST V3.4)* using a simple yet efficient linear regression approach to simulate kelp

22 canopies. An *in-situ* dataset of 2-1/2 years, with and without kelp forest coverage around Isla

23 Natividad (Baja CA, MX), allowed model validation for the main tidal constituents. *We tested*

24 *different* vegetation drag coefficients and compared simulations with our canopy model against

25 the standard vegetation module in *COAWST*. Results show that while both models simulate the

26 velocities observed in the *in situ* dataset reasonably well, our model better represents turbulence

27   kinetic energy through the water column as observed in laboratory experiments. This new kelp

28   model can be helpful in ecology, physics, and biogeochemistry studies.

1 INTRODUCTION

Kelp forest ecosystems occupy almost 7×10^6 km^2 globally, when accounting for polar regions of the world's coastlines (Duarte, 2017; Macreadie *et al*., 2019; Wernberg *et al.,* 2019), representing the largest coastal vegetated ecosystem in the world. Kelp lives in nutrient-rich habitats such as Eastern Boundary currents (EBUs) and provides significant global carbon sequestration either through respiration or carbon burial (Mcleod *et al.,* 2011; Britton *et al.,* 2016; Low *et al*., 2021, Eger *et al.,* 2023). While kelp forests are important for global carbon sequestration (Macreadie *et al*., 2019), kelp forests also have local biological (Gaylord *et al.,* 2002; Steneck *et al.,* 2003*)* and physical impacts (Gaylord *et al.,* 2007) that have been observed *in situ* (Walter *et al.,* 2012; Leary *et al.,* 2017; Monismith *et al.,* 2022) and in laboratory experiments (Rosman *et al.,* 2010; Rosman *et al.,* 2013). Considering that kelp forests have ecological, biogeochemical, and physical importance, comparative efforts to simulate these ecosystems in ocean models have been limited. Up to now, only one study has attempted to include the physical response of flows due to kelp forests into an ocean model, and it did not specifically account for variation in kelp canopy (Wu *et al.,*2017).

Kelp forests are found worldwide (Delille *et al.,* 2009; Schiel and Foster, 201t; Krause-Jensen *et al.*, 2016) and composed of 5 recognized types based on dominant genus: Ecklonia, Nereocystis, Lessonia, Laminaria, and Macrocystis (Rafaelli & Hawkins, 1999). Along the west coast of North America, the predominant species is the giant kelp *Macrocystis* spp. (Steneck *et al.*, 2002). *Macrocystis* spp. are found generally between 2 to 30 meters in the water column (Jackson & Winant, 1983) forming dense underwater forests (Steneck *et al.,* 2002) (Fig. 3.1). Kelp forests are recognized for their importance as shelter for macroinvertebrates, fish, and mammals (Dayton, 1985; Rafaelli & Hawkins, 1999). Furthermore, kelp forests greatly impact carbon storage or net

52   primary productivity (NPP). A kelp forest can uptake up to 4-fold more carbon per year than a

53   boreal forest (Reed & Brzezinski, 2009) or phytoplankton production in upwelling zones

54   (Behrenfeld & Falkowski, 1997). Kelp forests account for almost 5% of the total global blue

55   carbon and 1/3 of the total carbon sequestered in coastal regions (Filbee-Dexter & Wernberg, 2020;

56   Eger *et al.,* 2023). Similarly, kelp forests alter currents and mixing in subtidal nearshore

57   environments of temperate and high latitudes (Dayton, 1985; Rafaelli & Hawkins, 1999) and can

58   dampen headland upwelling processes (Valle-Levinson *et al.,* 2022).

59
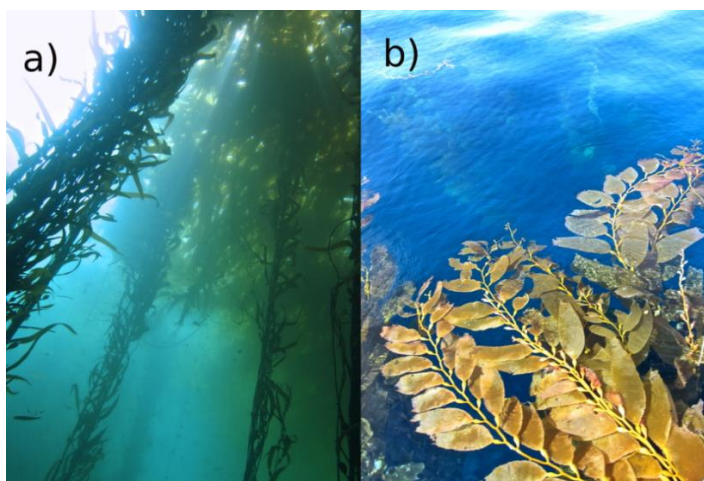
60

61   Figure 1 - Underwater formation of *M. Pyrifera* (a) and surface canopies at the surface (b). Source: Photos

62   taken by Charles Boch and modified by Matheus Fagundes.

63

64   Previous studies to understand the effect of kelp forests on currents focused on particular regions

65   along the California Current System (CCS; e.g: Jackson, 1984; Monismith *et al.,* 2022), scaled

66   laboratory experiments (e.g: Rosman *et al.,* 2010), or high-resolution simulation of kelp beds (e.g:

67   Wu *et al.,* 2017). While these studies helped better understand flow-vegetation interactions in these

68   complex ecosystems, they did not capture the entire range of effects that kelp forests have on the

69   biology, biogeochemistry, and currents. In this present study, a high-resolution semi-idealized

70   hydrodynamic model coupled with a vegetation module is used to create and validate a kelp

71   module to allow for studies on the effects of kelp forests, not only on the hydrodynamics, but also

72   the resultant effects on biogeochemical cycling and larval transport.

73   2 THEORY

74   The alongshore (v) momentum term of the Reynolds-Averaged Navier-Stokes (RANS)

75   equations under the Boussinesq approximation (Beudin *et al.*, 2017) can be written as:

76
$$\frac{\partial v}{\partial t} + \frac{\partial vu}{\partial x} + \frac{\partial vv}{\partial y} + \frac{\partial vw}{\partial z} + fu = -\frac{1}{\rho_0}\frac{\partial P}{\partial y} - \frac{\partial}{\partial z}(\overline{u'w'} - \nu\frac{\partial v}{\partial z}) + D_v + F_v \qquad \textbf{(1)}$$

77   where $\frac{dv}{dt}$ is the unsteady term, $\frac{d(uv)}{dx} + \frac{d(vv)}{dy} + \frac{d(vw)}{dz}$ are the advection terms, f is the Coriolis

78   parameter, $-\frac{1}{\rho_0}\frac{dP}{dy}$ is the pressure gradient in the y-direction, ρ_0 is the reference density of

79   seawater, $\overline{u'w'}$ is the vertical flux of horizontal momentum by turbulent velocity fluctuations, ν is

80   the molecular viscosity, D_v is the horizontal diffusive term, and the last term (F_v) is a forcing term

81   that includes the effects of vegetation on the flow. The spatially averaged vegetation drag force for

82   the alongshore velocity neglecting cross shore velocity can be written as:

83
$$F_{d,veg,v} = \frac{1}{2}C_d p d P_d \sqrt{v^2} \qquad \textbf{(2)}$$

84   Where P_d is plant density (plants m^{-2}), pd is the width of kelp (m) or diameter in the case of kelp,

85   and C_d is the drag coefficient for an individual plant. The code for the vegetation module in

86   *COAWST* was originally written to represent seagrasses, which do not extend to the water surface,

87   and therefore, no canopy was included. In these situations, the spacing between plants is constant

88   to the surface (Fig. 2a). However, kelp forests can have extensive canopies that cover the last meter

89   or so to the surface (Fig. 1; Traiger *et al.,* 2022). To date, the effects of surface canopies on currents

90 have only been studied in laboratory settings (Rosman *et al.,* 2013). However, kelp canopies can

91 be represented using a linear regression to allow individual plants to get closer together and the

92 kelp forest to become denser as the surface is approached (Fig. 2b). The second term important for

93 the development of our approach is plant thickness (*pt*). The *pt* is inversely proportional to the *pd*

94 in the second moment of area (*I*) equation ($=pdpt^3/12$) for the rectangle shape that was used by

95 Beudin *et al.,* (2017). While not ideal, we decided to keep the same equation for *I*.
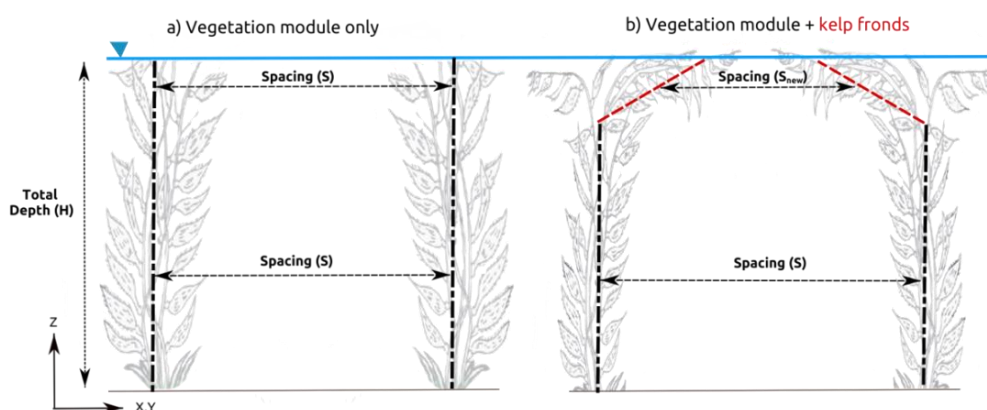
97 Figure 2 - Schematic of the two simulations in COAWST.

98 **3 METHODS**

99 **3.1 Kelp canopy module**

100 To account for kelp canopy, we developed a simple linear regression model that increases *pt* and

101 *pd* near the surface as:

$$
\begin{cases}
pt = pd = 0.3 & if \ depth \leq 12m \\
pt = pd = 2.3 * depth - 27.3 & if \ depth \leq 12m
\end{cases}
\tag{3}
$$

103 This modification in the vegetation model code captures the increase in kelp spacing (*S*) at the

104 surface between individual kelp plants. For our scenario, this gives *pt* and *pd* equal to 2.3 at the

105 surface, forming a virtually solid boundary. The coefficients in (3) can be varied to adjust for the

106   density, extent of the canopy, or water depth accordingly. The values reported are specific setup

107   to our model test case.

108   Two simulations are presented in this paper: The first simulation is running the *COAWST*

109   vegetation module with no changes (*standard* hereafter) (Fig. 2a), and the second is modifying the

110   code to account for kelp canopy (*canopy*) (Fig. 2b). The *standard* simulation assumes that *pd* and

111   *pt* are constant from the seafloor to the surface. The *canopy* simulation assumes a linear increase

112   in *pd* and *pt* in the last meter of the water column (Fig. 3.2; Utter & Denny, 1996). The *canopy*

113   module (eqn. 3) simulates the effects of kelp stipes and fronds getting close to each other (*S*) as

114   they spread out on the surface as they are longer than the water depth (Fig. 2b). The stipes and

115   fronds are then represented by changing *pd* and *pt* and, consequently, the effects of kelp forests on

116   the currents. These differences in *pd* and *pt* directly affect the bulk drag in the water column,

117   consequently changing the depth-averaged velocity and turbulence.

118   3.2 Area of Study

119   This study focuses on kelp forests surrounding Isla Natividad in the Vizcaino Bay region of Baja

120   California, MX. Baja California is affected by large scale forcings such as El Niño (Trenberth,

121   1997) and marine heat waves (Cavanaugh *et al.,* 2010; McPherson *et al.,* 2021). Mesoscale

122   forcings such as California Current characterized by low salinity, low temperature, high dissolved

123   oxygen (DO) and California Undercurrent (CU) that is saltier, higher temperature and low in

124   dissolved oxygen, also play a major role in the physical environment of this region (Mancilla-

125   Peraza *et al.,* 1993). Seasonally, there is a marked stratification in the upper 20 meters of the water

126   column, and conditions are influenced by wind-driven upwelling that brings water temperatures

127   as low as 8°C, salinity (~33.8), and low DO (<5.5 ml/l) to the surface during spring/summer.

128   During winter, waters can reach 16°C, salinity (~34), and DO around 5ml/l (Mancilla-Peraza *et*

129   *al.,* 1993). Around Isla Natividad, winds, waves (surface and internal), tides, and kelp forests drive

130   the dynamics (Woodson *et al.*, 2018; Valle-Levinson *et al*., 2022) at relatively small spatial and

131   temporal scales (e.g: < 1 km, < 24 h). For instance, the shape of kelp forests can modify tides and

132   dampen headland upwelling (Valle-Levinson *et al*., 2022).

133   Isla Natividad is a 7 km long island south of Isla Cedros in Central Baja California, Mexico

134   (Schlenger *et al.,* 2021) located between 115°15'W-115°6'W and 27°48'N-27°55'12''N (Fig. 3).

135   The island is bounded by Kellet Channel on the north and Dewey Channel on the south (Mancilla-

136   Peraza *et al.,* 1993), and is surrounded year-round by kelp forests (*Macrocystis Pyrifera*) which

137   provide shelter for organisms including abalones (*Haliotis* spp.; Micheli *et al.,* 2012). Isla

138   Natividad has two distinct local ocean regions on each side of the island (Woodson, 2018). On the

139   southeastern side, Morro Prieto can reach mean temperature of 16°C and mean DO of 6 mg/l at 12

140   m while on the northwestern side, Punta Prieta has waters that are typically 3°C warmer and mean

141   DO of 7.5 mg/l (Boch *et al.,* 2018) at the same depth. Because of the economic and ecological

142   importance of abalone, the fishing cooperative, Buzos Y Pescadores, in Isla Natividad established

143   2 marine reserves that have been monitored since 2006 (Boch *et al.,* 2018; Micheli *et al.,* 2012).

144   One of the marine reserves is located near Punta Prieta and has oceanographic sensors (CTDs,

145   MiniDOTs, thermistors, and adps) at 7 m and 12 m depth (Boch *et al.,* 2018)**.**

146

147

148

149
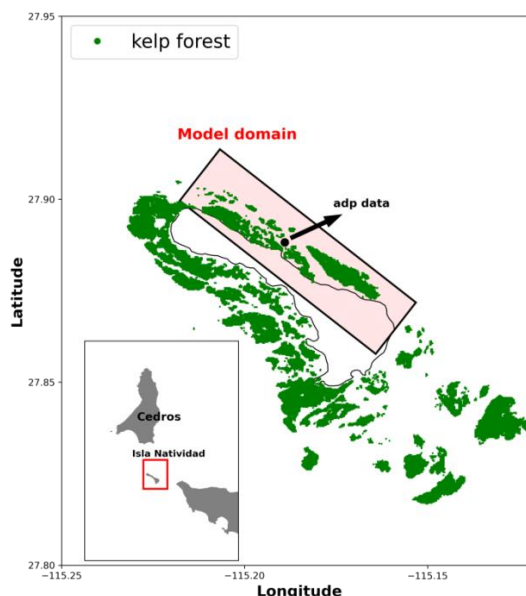
150

151   Figure 3 - Map of Isla Natividad indicating regional location and areas covered with kelp. Black circle

152   indicates location of adp data used in this study. Punta Prieta, on the northeastern side of Isla Natividad.

3.3 Forcing

154   The mooring at Punta Prieta (Fig. 3) was chosen for evaluating the vegetation models in

155   *COAWST* for four reasons, a) long-term data are available (Woodson, 2018), b) a heat wave in

156   2015-16 complete removal of kelp (Fig. 4) allowing understanding the environment without kelp

157   (Monismith et al 2022), c) it is within a marine reserve thereby providing a relatively undisturbed

158   habitat (Micheli *et al.,* 2012), and d) flows are generally tidal and alongshore in contrast to flows

159   around Morro Prieto (Boch *et al.,* 2018).
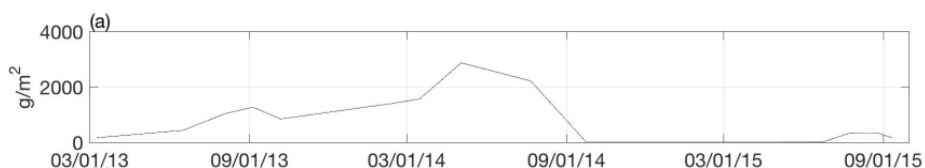
160

161   Figure 4 - Averaged kelp biomass around Isla Natividad, MX. Source: Monismith et al., 2022.

162

163   *In situ* current data were collected every 0.5 meter starting from 0.65 meters above the bottom to

164   the surface (~14 m) from 2013-2016 using a 1MHz Nortek Aquadopp (*adp*; Fig. 3.5). The depth

165   of the adp data used for this simulation was from 2.65-12.65 meters from the bottom to remove

166   errors in the first couple of meters due to sidelobe interference (Lentz *et al.,* 2022). Depth-averaged

167   velocities were calculated after removing errors from bottom and surface (Supplementary Fig. 1).

168   Both E-W and N-S velocities increased in the 2015 period (Supplementary Fig. 1) when there was

169   no kelp biomass observed (Fig. 4) while in 2014, the highest kelp biomass observed for the 2-1/2

170   year record, velocities were ~2-fold slower (Monismith *et al.,* 2022).

171   Currents were rotated into along- and cross-shore axes using Principal Component Analysis

172   (PCA; Campbell & Atchley 1981; Emery & Thompson 2004). The rotated velocities were

173   separated by season (Fig. 5). Based on Fig. 4 and Fig. 5, the cross-shore and alongshore Winter

174   2015 (henceforth *adp*15) and Spring 2014 (*adp*14) velocity records are used for no-kelp and kelp

175   analyses. The adp15 data set was used to validate *COAWST* without the vegetation module before

176   implementing it for the adp14 dataset (e.g., to estimate drag coefficients in the absence of kelp).

177

178
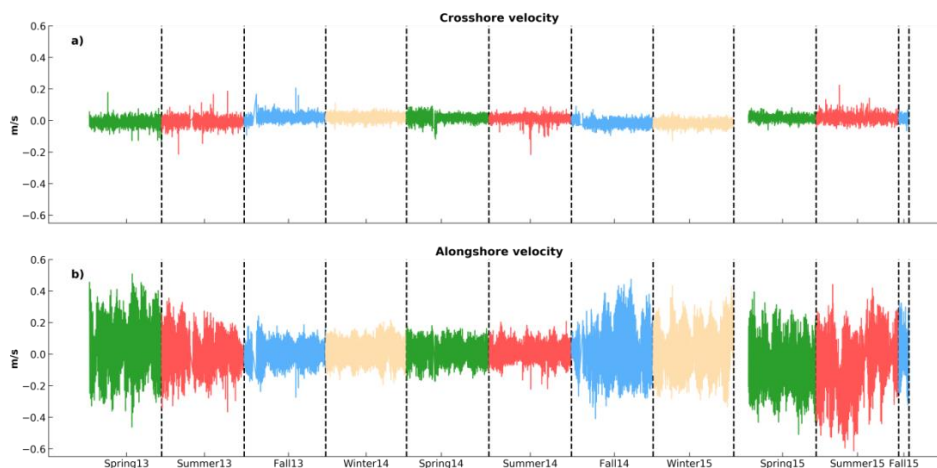
179

180   Figure 5 - Rotated cross-shore and alongshore velocities separated by season.

181

182 Both, cross-shore and alongshore velocities from adp15 and adp14 were harmonically analyzed

183 using a python version of T-TIDE (Pawlociwicz *et al.,* 2002**;** Figs. 3.7, 3.8**)** before being used to

184 force *COAWST* and to validate the vegetation module, respectively.

185   3.4 Numerical Model Description

186   The model used in this study was the *Coupled Ocean-Atmosphere-Wave-Sediment-Transport*

187 *model (COAWST V3.4*; Warner *et al*., 2008). The ocean component of *COAWST* is the *Regional*

188 *Ocean Modeling System (ROMS)* (Haidvogel *et al.,* 2008). ROMS is a 3-D, free-surface model

189 that solves the primitive equations using hydrostatic and Boussinesq approximations with

190 topography-following sigma layers (Shchepetkin and McWilliams, 2005; Haidvogel *et al.,* 2008).

191 For the momentum equations, splines vertical advection and logarithmic bottom friction were

192 selected to keep stability and better represent the environment, respectively. The model used the

193 Mellor-Yamada level 2.5 turbulence closure scheme (MY-2.5). All boundaries (N,S,E,W) allowed

194 along- and cross-shore flows. A periodic boundary condition was applied for free-surface, a Flather

195   condition for 2D u- and v-momentum, and a Radiation-Nudging condition for 3D u- and v-

196   momentum.

197   The barotropic time-step was set at 10 s. Bottom roughness (z_{ob}) was 0.03 m and surface

198   roughness (z_{os}) was 0.4 m with a no-slip condition along the bottom to provide a best fit for the

199   no-kelp simulations to observed velocity profiles. The model had 40 sigma-layers splitting the 13

200   meters of water column with surface stretching (θ_s) = 1, bottom stretching (θ_b) = 2, and thermocline

201   depth (Tcline) = 0. The domain was approximately 14 km long by 3 km wide (Fig. 6) with a grid

202   size of 25 meters x 25 meters. The model was initialized at rest with a well-mixed domain where

203   temperature and salinity are 19°C and 34, respectively (Low *et al.,* 2021). The model was forced

204   every 10 min with depth-averaged tidal fits from adp15 (Monismith *et al.,* 2022). Hydrodynamic

205   conditions of the domain were simulated for three months. However, the first 30 days provided

206   dynamic adjustment of the currents. The vegetation module was activated, accounting for the drag

207   due to the kelp forests in the simulations using the *standard* and *canopy* modules (Beudin *et al.*,

208   2017), and the flexibility flag (VEG_FLEX) was turned off for both scenarios. Results are

209   presented for the second month of each simulation.

210
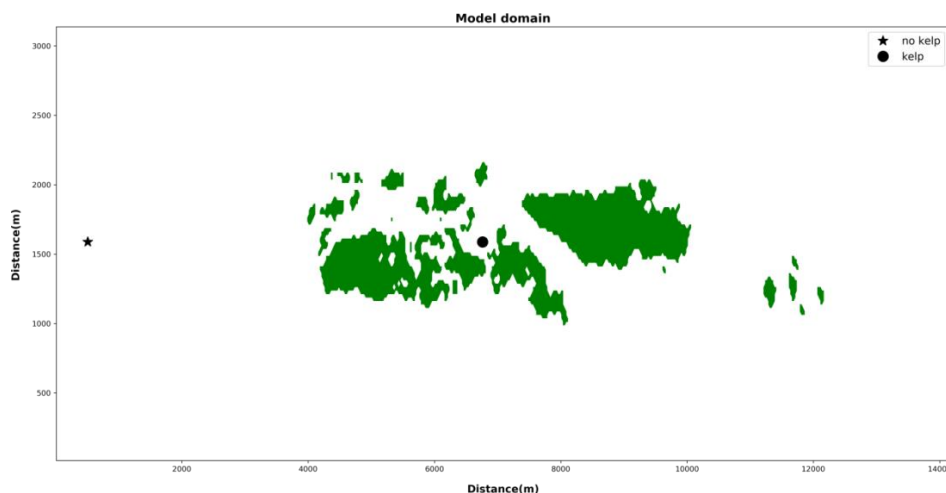
Figure 6 - Model domain. No kelp station (star) is used to validate the idealized model and kelp station

(circle) is used to validate the vegetation module in *COAWST*.

3.5 Vegetation module parameters

The vegetation module is a standard component in *COAWST* (Beudin *et al.*, 2017). This module

receives u and v from *ROMS* and returns both the drag force (F_d) and vertical turbulent mixing

(Beudin *et al.*, 2017). The vegetation module requires 4 parameters: plant height (m), plant density

(plants/m^2), plant diameter (m), and plant thickness (m) (Table 1). The other settings are number

of vegetation types, Young's modulus (10^7), vegetation mass density (1000.0), additional

horizontal viscosity coefficient (0.0), and drag coefficient for each individual plant (0.05-0.6).

226   Table 1 - Vegetation module initial parameters.

	Plant height(m)	Plant Density (plants/m²)	Plant diameter (m)	Plant thickness (m)
Standard	13	0.9*	0.3	0.3
Canopy			See equation 3	See equation 3

227   *(GAYLORD *et al.*, 2007).

3.6 Time-averaged velocity

229   The output velocity data were used to calculate the time-averaged velocity ($\bar{u}$). To compute $\bar{u}$,

230   alongshore and cross-shore velocities were used to calculate velocity component in the domain,

231   and then, integrated in time:

$$|V| = \sqrt{\bar{u}^2 + \bar{v}^2} \qquad \textbf{(4)}$$

$$\bar{u} = \frac{1}{T}\int_0^T u\,dt \qquad \textbf{(5)}$$

3.7 Model Skill

235   A quantitative model skill was presented by Willmott (*1981*) (eq. 6)*:*

$$WS = 1 - \frac{\sum_{i=1}^{N}(m_i - o_i)^2}{\sum_{i=1}^{N}(|m_i - \bar{o}| + |o_i - \bar{o}|)^2} \qquad \textbf{(6)}$$

237   where *m* is the variable modeled being compared against the observed variable (*o*), the index *i*

238   represents each depth for our case. It takes the sum of difference for each point squared and divides

239   by sum of the absolute variability of the model and observed variable in relation to the mean of

240   the observed variable squared. A Willmott Skill equal to 0 (WS = 0), means complete

241   disagreement, and, *WS* = 1 means exact match between simulations and observations. This

242 verification has been applied in other model simulations (Warner *et al.,* 2005b; Liu *et al.,* 2009).

243 Before calculating *WS*, the model was interpolated to the depths of the *adp* dataset. Time-averaged

244 velocities for the domain with the vegetation module off and the *no kelp station* (Fig. 6) were the

245 same, and therefore, we used *no kelp station* for the validation. The *kelp station* (Fig. 6) was used

246 and compared against *adp*14 where kelp biomass was the highest (Fig. 4).

3.8 Bulk Drag calculations

248 Field estimates of kelp forest drag coefficients represent the bulk drag effect of multiple kelp

249 plants. For example, in a 1-D linear momentum balance,

$$\frac{\partial u}{\partial t} + C_D^B \frac{U\,|U|}{h} = -g\frac{\partial \eta}{\partial x} \qquad \textbf{(7)}$$

250

251 After some manipulation:

$$C_D^B = -\frac{h(\frac{\partial u}{\partial t} + \frac{\partial \eta}{\partial x})}{U\,|U|} \qquad \textbf{(8)}$$

252

253 Applying the centered difference method for $\frac{\partial u}{\partial t}$ and $\frac{\partial \eta}{\partial x}$, yields:

254

$$C_D^B = \frac{-\frac{h}{2\Delta t}(u_j^{t+1} - u_j^{t-1}) - \frac{hg}{2\Delta t}(\eta_{j+1}^t - \eta_{j-1}^t)}{\bar{u}\,|\bar{u}|} \quad \textbf{(9)}$$

255

256 The bulk drag coefficient, C_D^B (eq. 9), is the net coefficient for the entire region of influence, which

257 is not necessarily the drag force on an individual kelp plant, C_D^i. In the *COAWST* model, the drag

258 coefficient input is for an individual plant, C_D^i. Therefore, to evaluate model input, we changed C_D^i

259 and used the model to estimate C_D^B. Computing C_D^B does two things, 1) shows that the drag on an

260 individual kelp plant is not the same as the bulk drag coefficient, and 2) allow us to parameterize

261 the kelp model. In total, there were 12 simulations varying C_D^i from 0.05 to 0.6. A threshold for

262   velocities less than 0.05 m/s was imposed in order to get reasonable estimates of C_D^B during

263   calculations.

3.9 Turbulent Kinetic Energy (TKE)

265   Turbulent kinetic Energy (TKE) is generally described by the intensity of the turbulent motion.

266   The nearshore environment is believed to be an important region that dissipates TKE (Carter *et*

267   *al.,* 2005). Like bottom boundary conditions in a nearshore environment, vegetation also increases

268   TKE (Rosman *et al.,* 2010; Kalra *et al.,* 2017). For example, a laboratory study demonstrated that

269   while kelp increased TKE in the water column when compared to no kelp, the largest turbulence

270   occurred when the kelp had a dense surface canopy (Rosman *et al.,* 2010). TKE was calculated by

271   *ROMS* and normalized by the total velocity. The TKE calculation was computed only for a cross-

272   section area where kelp forest region was present.

4 RESULTS

274   Before starting the analysis of the kelp forest model, the model needs to adjust to a stable

275   condition using a spin-up period to remove transient dynamics due to initial startup. For this

276   simulation, we use sea surface elevation as the spin-up variable (Fig. 7). Because the no kelp

277   simulation only has alongshore and cross-shore velocities as forcings, the period needed to

278   stabilize was a little less than a month (Fig. 7-a), when kelp was added the spin-up period increased

279   to closer to a month (Fig. 7-b). The amplitude of the sea surface height (SSH) stayed at 0.02 m and

280   0.001 m for no kelp and vegetation module on, respectively. There was no difference in SSH

281   amplitude and time for the system to stabilize for both simulations *standard* and *canopy*. When

282   the vegetation module is added, SSH amplitude decreases, representing up to 40% reduction in

283   amplitude.

284

285
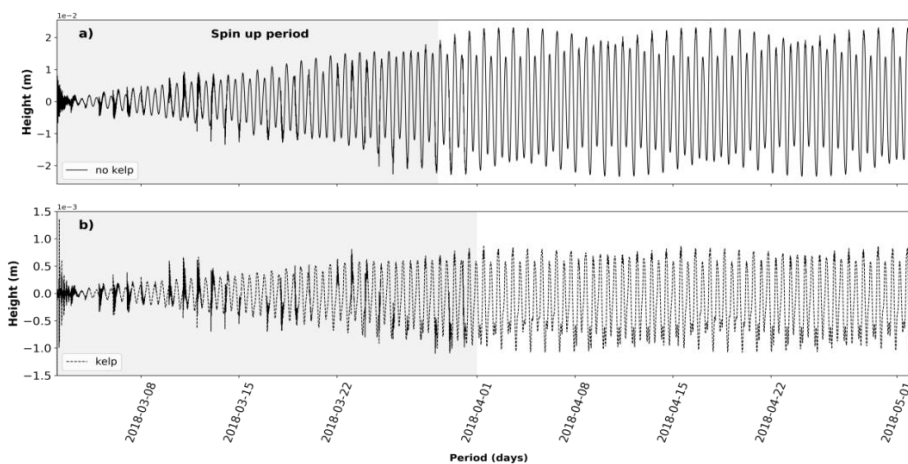
Figure 7 - Spin-up of the model domain for no kelp and inside kelp.

286

287

288   For the remaining analysis, the model was interpolated to the points of the *adp* dataset. The no

289   kelp model showed good agreement with *adp15* (Fig. 8). Validation of the time-averaged currents

290   was only possible up to 10.15 m from the bottom due to invalid values measured by the *adp15*

291   instrument. The model overestimated the velocity over the first 4 m, underestimated it up to 9 m,

292   and overestimated for the remainder of the data available. The absolute maximum difference was

293   0.008 m/s between model velocity and those observed at 6 m. The skill for the time-averaged

294   velocity in the no kelp model run compared to *adp15* was 98.8%. A high *WS* indicates a good

295   agreement with the variability of the observed dataset.

296

297
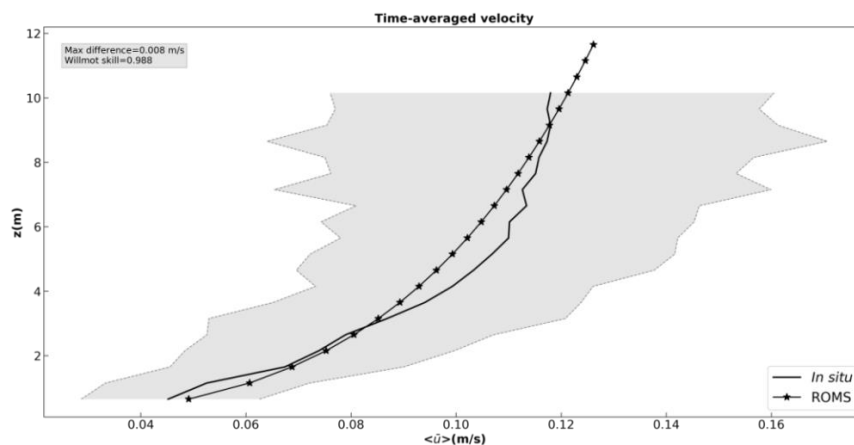
Figure 8 - Time-averaged profile comparison between *adp* data and model run without *vegetation* model.

The gray region shows the 95% CI and mostly represents variation in velocity due to tides. Y-axis is above

the bottom.

301

For both configurations with kelp, modeled time-averaged velocities decreased with increased

$C_{d,veg}$ as expected (Fig. 9). The *standard* configuration showed a slightly higher time-averaged

velocity than *canopy* throughout all case scenarios. This difference was more pronounced in the

last 4 m to the surface. $C_{d,veg}$ was a way to change the fit of the velocities in the kelp simulation.

Changes of 0.05 for $C_{d,veg}$ were considered a safe and fast approach to fit the best scenario while

not having to simulate too many scenarios. The best fit scenarios were $C_{d,veg} = 0.35$ (Fig. 9-g) and

$C_{d,veg} = 0.4$ (Fig. 9-h) for the *canopy* and *standard* models, respectively. At $C_{d,veg} = 0.35$, the

standard model provided a better fit between 7-9 m than the *canopy* but overestimated everywhere

else compared to the new model. This was different for the $C_{d,veg} = 0.4$ scenario. While the *canopy*

model showed a slightly better fit in the first 5 meters from the bottom, the overall best fit was

modeled using the *standard* approach. The higher value for the *standard* module also represents

the effect of not applying the effects of the kelp canopy over the entire water column.
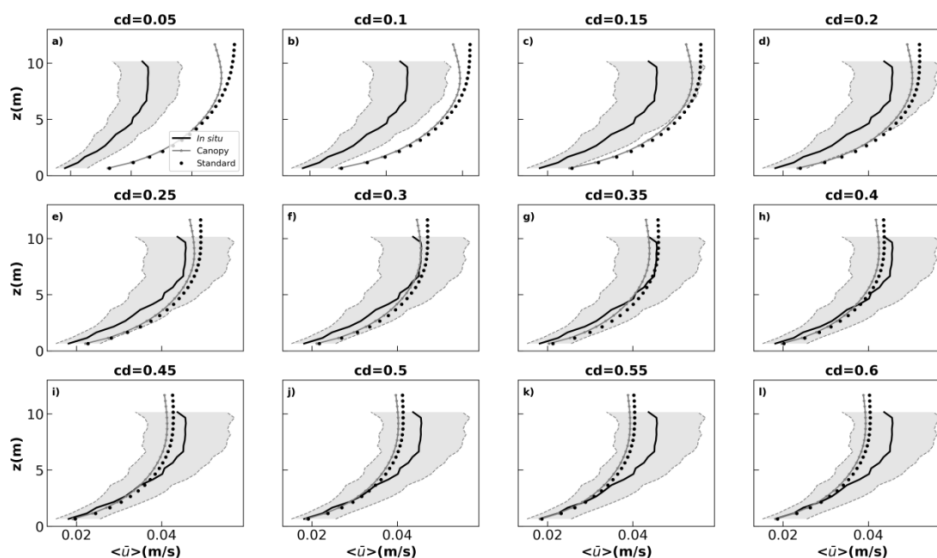
Figure 9 - Time-averaged profiles comparison between *adp* data and for standard and canopy. The gray

region shows the 95% CI for the effects of the tides. Y-axis is above the bottom.

Table 2 shows *WS* calculated for the best $C_{d,veg}$ of each configuration. The water column was

divided into upper and lower regions for this assessment to understand the impact of the code

modification but also assess over the entire water column to check the overall fit. The division at

5 m was done because the *in-situ* data only extends to 10 m. Over the entire water column *WS* was

similar. Between the two regions, both simulations had greatest skill in the first 5 m which is

observable in Fig. 9g-h. The *standard* model was slightly better near the bottom. The largest

difference was observed in the upper 5 m, where *canopy* model had the most skill (*WS* = 0.767).

This difference is due to a slightly better fit between 5-6 m and between 8-9 m, where the velocity

still feels the canopy acting on the surface velocities.

328   Table 2 - WS for the two best vegetation drag for both standard and canopy models.

	*top**	*down***	*total****
Standard	0.721	0.972	0.983
Canopy	0.767	0.967	0.983

329
330   * Calculated using values where depth is greater than 5. ** Calculated using values where depth is less or equal 5. ***Calculated for all the water column.

331

332   *WS* scores separated by 0.01 m/s bins are shown in Fig. 10. Both *canopy* and *standard* simulate

333   similar along- and cross-shore velocities when compared against *in situ* datasets. *WS* values range

334   from 0.25-0.93 for alongshore velocities (Fig. 10a) and 0.19-0.47 for cross-shore velocities (Fig.

335   10b). As expected, alongshore *WS* showed better comparison than cross-shore. One possible

336   reason is that cross-shore velocities at the Punta Prieta site are also affected by internal waves and

337   tides, while surface tides dominate alongshore velocities. As a result, alongshore velocities

338   compare better with observations at higher velocities than velocities closer to zero where there can

339   be more uncertainty in both the model and measured velocities. Cross-shore velocities are best

340   simulated between 0.04 and 0.05 m/s.

341

342

343
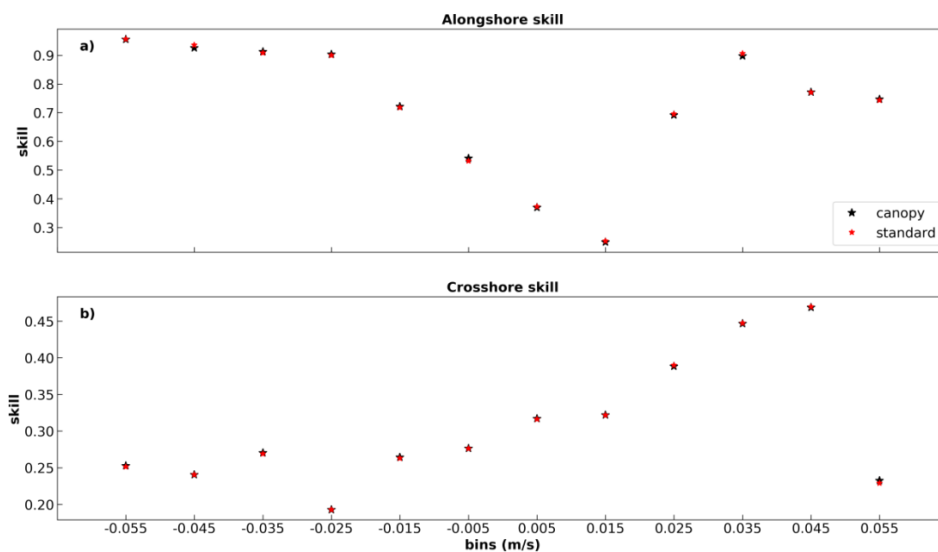
Figure 10 - WS for alongshore (a) and crosshore (b) for canopy and standard simulations split by 0.01 m/s

345   bins.

346   Median bulk drag (C_D^B) increased as vegetation drag ($C_{d,veg}$) increased for both simulations (Table

347   3). The variability also increases as $C_{d,veg}$ becomes large. The C_D^B calculated for *canopy* is slightly

348   larger for all $C_{d,veg}$ used. C_D^B for the best simulations were the same 0.084 and had the same

349   variability ± 0.072. These values are within the values for dense kelp forests ($C_D^B = 0.18$) and sparse

350   kelp forests ($C_D^B = 0.07$) in a laboratory study (Rosman *et al.,* 2010). The values were also in

351   agreement with Monismith *et al.,* (2022) for the *adp*15 data used for this simulation ($C_D^B \sim 0.04$).

352

353

354

355

356

357 Table 3 - Median bulk drag coefficient and 95% CI calculated from **equation 7** for *standard* and *canopy*.
358

	Cd_{veg} = 0.05	Cd_{veg} = 0.10	Cd_{veg} = 0.15	Cd_{veg} = 0.20	Cd_{veg} = 0.25	Cd_{veg} = 0.30	Cd_{veg} = 0.35	Cd_{veg} = 0.40	Cd_{veg} = 0.45	Cd_{veg} = 0.50	Cd_{veg} = 0.55	Cd_{veg} = 0.60
Standard$_{cd}$	.032± 0.016	.048± 0.028	.060± 0.037	.067± 0.045	.073± 0.052	.078± 0.059	.082± 0.065	**.084± 0.072**	.087± 0.078	.090± 0.084	.092± 0.090	.095± 0.093
Canopy$_{cd}$	.036± 0.018	.052± 0.030	.064± 0.040	.071± 0.048	.077± 0.056	.081± 0.063	**.084± 0.070**	.087± 0.077	.090± 0.085	.093± 0.091	.096± 0.094	.098± 0.094

359

360   The estimates of bulk drag (C_D^B) improves as Reynolds number (Re) increases (Fig. 11). Depth-

361 averaged velocity was binned from 0.01 m/s to 0.09 m/s with 0.01m/s intervals. C_D^B also has a Re

362 dependency as expected. The medians for the two models are not statistically different. The C_D^B

363 estimations are higher and less precise for smaller Re values (e.g: $10^{5.5}$ to $10^{5.8}$), and as the depth-

364 averaged velocity increases bulk drag estimates are closer to what has been observed in the

365 literature (Rosman *et al.,* 2010; Monismith *et al.,* 2022).

366   While the time-averaged profiles and bulk drag estimation are similar between both models, the

367 difference in the mean velocity and its variability observed from the last two meters to the surface

368 is quite different (Fig. 12). Overall, the largest differences are on the edges of the kelp forest region.

369 The *standard* model had higher velocity and variability than *canopy* model in the last 2 m near the

370 surface (Fig. 12a-b), resulting from the addition of kelp canopy in the latter model. *Canopy* had

371 slightly higher velocity just below the kelp canopy especially on the edges (Fig. 12a). This decrease

372 in time-averaged velocity at the surface and an increase at the bottom has been previously observed

373 in laboratory for dense kelp with canopy (Rosman *et al.,* 2010; Rosman *et al.,* 2013).

374
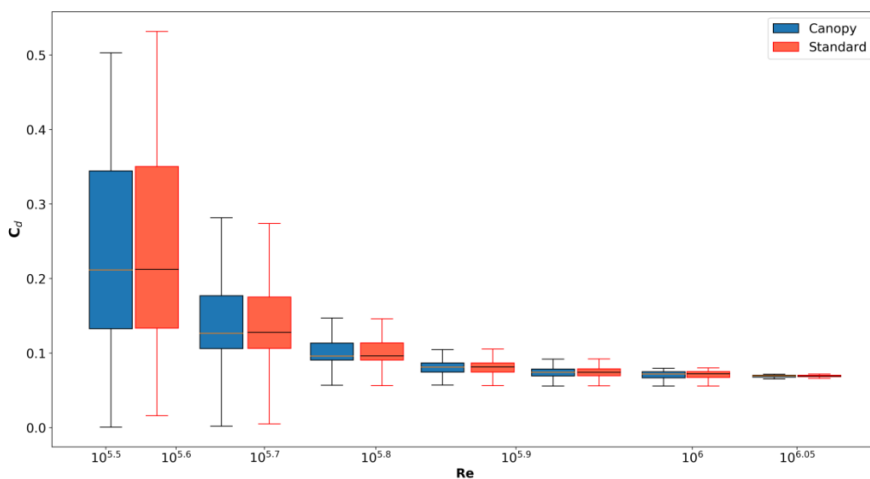
375

376   Figure 11 - Bulk drag versus Reynolds number for depth-averaged velocities at each 0.01m/s interval for

377   both canopy and standard.

378

379
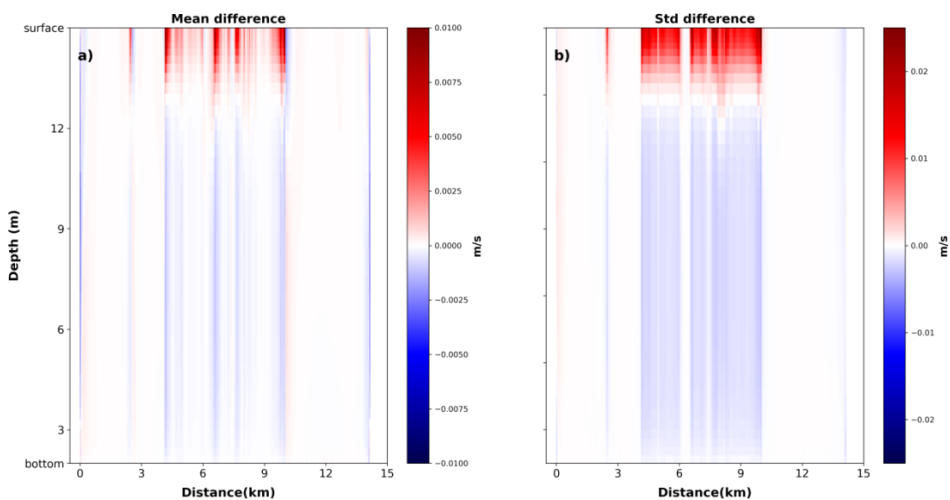
380

381   Figure 12 - Mean (a) and standard deviation (b) of velocities difference between standard and canopy.

382   Alongshore slice at 1500m.

383

384   Absolute time-averaged cross-shore (Fig. 13a) and alongshore (Fig. 13b) velocities for the

385   canopy simulation illustrate the ducting of flow around patches of kelp (Valle-Levinson et al

386   2022). Velocities in the kelp were disregarded, and where kelps are present in the model are shown

387   in brown. There is an increase in mean time-averaged cross-shore speed along the outer and inner

388   edges of the kelp forest (Fig. 13a). The highest absolute cross-shore velocities are located between

389   kelp forests at 6.8 and 7.4 km. Flow acceleration along the edges of kelp forests has been

390   previously observed (Jackson & Winant, 1983; Jackson, 1998; Graham, 2003). In addition, the

391   flow channeling between kelp gaps has been described recently for the same region (Valle-

392   Levinson *et al.*, 2022). The absolute time-averaged alongshore speeds decrease to almost zero

393   between 1 and 1.5 km (Fig. 13b). The giant patch in front of this section is the cause of these

394   velocities being almost null. The alongshore section shows flow channeling between 1.5 and 2 km.

395   Flow channeling is stronger closer to the 2 km region and for depths between 8.5 m and the surface.

396   Velocities are higher on the outer edge (approximately at 2.2 km) where there is no large patch

397   that inhibits flows in that area. As a result, our model could also be applied to understand the

398   effects on nutrient uptake (Gaylor *et al.*, 2007), larvae dispersal (Graham, 2003), and connectivity

399   among beds (Gaylord *et al.*, 2006). In addition, Valle-Levinson *et al.*, (2022) hypothesized that

400   these regions could provide localized sites of fertilization and safe spaces for various species.

401
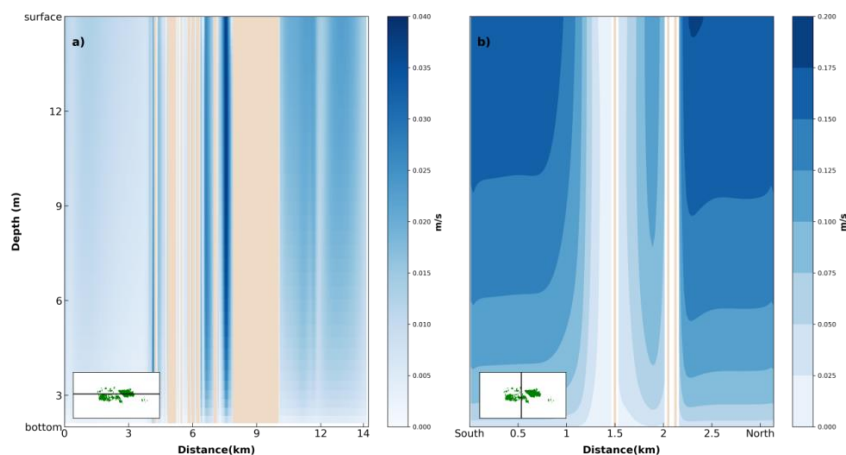
402

403   Figure 13 - Absolute time-averaged cross-shore (a) and alongshore (b) velocities for canopy module

404   simulation. Brown region indicates where kelp forest module is present in the model.

405

406   Profiles of normalized TKE (hereafter TKE) for *standard*, *canopy*, and canopy with 50%

407   coverage (instead of 100%) at the surface (*canopy50*) further illustrate the effects of kelp canopy

408   on flows (Fig. 14). TKE was relatively the same from 0.5 m up to 7 m above the bottom for both

409   the *standard* and *canopy* models. The *standard* profile is close to a linear function as expected for

410   free surface flows. Similar mean TKE profiles were observed for no kelp and no canopy scenarios

411   in a laboratory experiment (Rosman *et al.,* 2010). The *canopy* simulation showed a TKE peak 2-

412   fold higher than Rosman *et al.* (2010) while *canopy50* showed values similar to this laboratory

413   study for a dense canopy scenario. We believe this is because of the spacing at the surface in the

414   *canopy* scenario acting as almost a solid boundary at the surface generating more friction, and

415   therefore, more TKE. While the profiles in the Rosman *et al.* (2010) do not show the bump

416   observed in the simulations, we observed that the peaks, for both sparse and dense with kelp fronds,

417   are always deeper than the actual kelp fronds located at the surface which is also observed in both

418   simulations *canopy* and *canopy50*. TKE then decreases within the canopy.

419
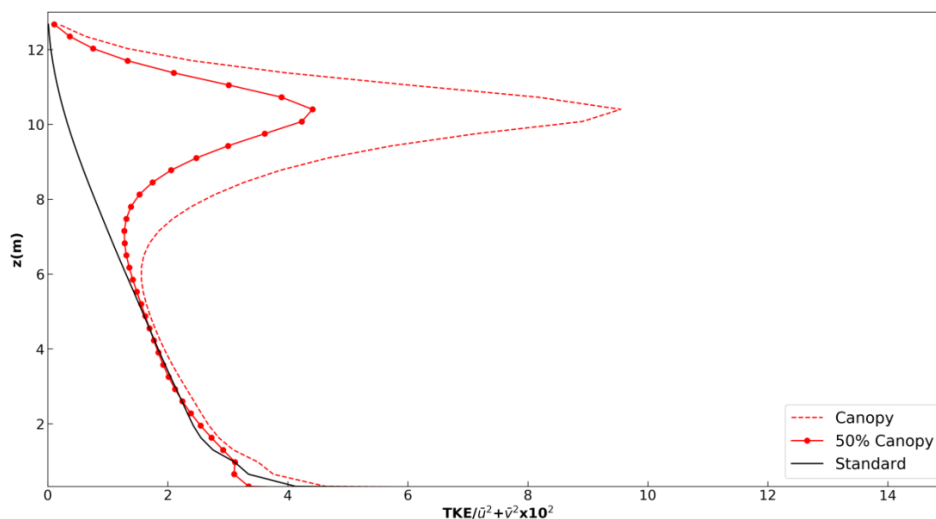
Figure 14 - Averaged normalized TKE only in the kelp forest region. Alongshore slice at 1500m.

421

5 DISCUSSIONS

The Coupled Ocean-Atmosphere-Wave-Sediment transport (*COAWST*) modeling system has been successfully applied to characterize wave-flow-seagrass interactions (Beudin *et al.*, 2017). The new module described in this paper, expands *COAWST* capability to simulate flow-vegetation interactions for canopied vegetation, specifically kelp forests. This module not only simulates the time-averaged tidal-driven currents in the presence of kelp forests but also the wake (turbulent kinetic energy) generated by kelp fronds as observed in laboratory experiments (Rosman *et al.,* 2010).

The influence of kelp forests on currents have been modeled previously (Wu *et al.,* 2017; Frieder *et al.,* 2022). However, these models did not explicitly account for the presence of a canopy or were run offline and thus did not provide feedback to the regional model. In this study, we implemented changes in flow and turbulence caused by kelp forests in a regional ocean model that

434   provide feedback on the flows themselves. This was possible because of the vegetation module

435   developed by Beudin *et al.,* (2016) and our modifed approach to simulate kelp canopy. In a

436   previous study, the effects on currents by the drag generated due to kelp forests was only

437   implemented at the bottom of the domain (Wu *et al.,* 2017). Like this study, they also observed

438   damping in the tidal velocity for regions where kelp beds were present. The most recent study

439   documenting kelp forest simulation (Frieder *et al.,* 2022) not only added the changes in the flows

440   in the water column but also simulated growth and death of kelp forests, making their model more

441   robust than the one present here for simulating kelp effects over longer time frames. However, the

442   shortcoming of their model was that they used an offline Large Eddy Simulation (LES) forced by

443   model outputs, and therefore, no direct feedback in the regional ocean model. While we understand

444   our kelp forest simulation uses a static kelp forest domain and does not show a more realistic kelp

445   forest seasonal cycle, it does represent well the domain when kelp density is zero and when kelp

446   density is high (0.9 plants/m^2). This module can be expanded to be used to understand the two way

447   interaction between kelp forests, currents, and biogeochemistry, for example, and could be

448   modified to vary parameters through time to account for growth and decay of kelp forests over

449   seasonal and interanual cycles.

450   The module presented here shows good agreement for the time-averaged velocity at Punta Prieta

451   for the 2015 period when kelp was absent (Monismith *et al.,* 2022). The differences observed

452   mainly in the middle of the water column between our model and the *in situ* dataset could have

453   been because the simulation was only forced with the two main tidal constituents for the domain

454   and did not include wind and wave effects on currents (Monismith *et al.,* 2022). However, while

455   the largest difference between model and *in situ* dataset occurs in the middle of the water column,

456   we believe this difference could be due to two possible issues: a) model settings, for example, the

457   sigma layers being coarser in the middle of the water column, or b) not having a solid coast on the

458   south boundary representing the island which could change the cross-shore velocities in the water

459   column (Russell & Vennell, 2017). The upper 2 m of the water column cannot be compared due

460   to *adp* instrument capabilities pointed out by Monismith *et al.,* (2022). This upper 2 m is strongly

461   influenced by winds and waves that increase the velocity (see Fig. 7 in Monismith *et al.,* 2022)

462   and for our case we did not consider these two other processes.

463   When kelp is present, time-averaged velocity profiles show a rapid decrease in the last meter to

464   the surface. Neither the *standard* nor *canopy* modules captured the change in the last 2 m of the

465   water column observed in the *in situ* datasets. When kelp is present at the Punta Prieta site, the

466   velocities are wave-induced (Monismith *et al.,* 2022). This forcing is not imposed in the domain.

467   Consequently, both models simulate similar patterns up to 10 meters by changing the vegetation

468   drag by only 0.05. However, even if measurements for the last two meters are unreliable, we

469   observe that the in situ data tends to slow down in the canopy region. The canopy region is formed

470   due to the spread out of kelp fronds in the upper 2 m (Jackson, 1984), resulting in a dense region

471   with larger drag than the rest of the kelp environment (Rosman *et al.,* 2010), almost like a semi-

472   wall. Although, our *canopy* approach does not account for changes in kelp orientation with

473   currents, it shows better results in the canopy region than the *standard* module (Fig. 12h).

474   The nearshore environment is believed to be a region that dissipates TKE (Carter *et al.,* 2005).

475   Like bottom boundary conditions in a nearshore environment, vegetation increases TKE (Rosman

476   *et al.,* 2010; Kalra *et al.,* 2017). For example, kelp forests significantly affect the various physical,

477   chemistry, and biological processes due to the turbulence near the canopy region (Rosman *et al.,*

478   2010). To our knowledge, this is the first time a hydrodynamic model was able to model TKE in

479   the water column caused by canopies.

480   The density of *M. pyrifera* plants varies significantly throughout the year (Monismith *et al.,*

481   2022). Reed *et al.,* (2009) found that the lowest densities were during the end of winter season

482   while the highest were during summer. The same authors found that the spacing between canopies

483   decrease to its minimum during fall and increase during winter. For our simulations, we found that

484   plant density ~ 0.9 plants m^{-2} (Gaylord *et al., 2007;* Reed *et al.,* 2009) and *canopy50* produced the

485   best scenario for summer periods, and therefore, the best fit to TKE estimates. Consequently, a

486   study to develop a time-varying change in canopy spacing is needed to understand the impact of

487   fronds for seasonal and yearly variability in kelp domains. Nonetheless, this new module opens

488   opportunities to study how TKE affects nutrient availability (Rosman *et al.,* 2010), oxygen

489   dynamics (Murie & Bourdeau, 2020), and larval transport (Pakhomov *et al., 2022*) in kelp forest

490   regions.

491   6 CONCLUSIONS

492   The *canopy* method presented in this paper to simulate kelp forests including the canopy is a

493   new and relatively simple way to represent kelp forests in *COAWST*. The module modifies the

494   plant thickness and plant diameter to decrease spacing in the last meter of the water column to

495   mimic the effects of the kelp canopy. The revised module slightly improved fits to velocity and

496   greatly improved fits to TKE depth profiles over the default vegetation module provided in

497   *COAWST*. Although both the canopy and standard modules produced comparable time-averaged

498   velocity profiles compared to the *in-situ* data, the presence of the kelp canopy resulted in a marked

499   enhancement of turbulence near the surface. Such an improvement could considerably influence

500   air-sea fluxes, biogeochemical processes, and the distribution of larvae within the kelp forest. This

501   model provides improved opportunities to study the impacts of kelp forests around flows and can

502 further be used to understand larvae dispersal and biogeochemistry in a kelp environment using

503 hydrodynamic models.

Code availability

505 The modified code for the **canopy** module and the codes to generate the data and figures are
506 available at https://doi.org/10.5281/zenodo.10160564 (Fagundes and Woodson, 2023). The
507 COAWST V3.4 source code is available from https://github.com/CSOMIO/COAWST (last
508 access: Nov, 27th, 2023)

Author contributions

510 C.B.W. designed the study. M.F. conducted model runs. M.F. and C.B.W. analyzed the data. F.M,
511 S.G.M, A.V.L. contributed significantly with constructive feedback to the science and internal
512 discussions of the manuscript.

Disclaimer

514 Publisher's note: Copernicus Publications remains neutral with regard to jurisdictional claims in
515 published maps and institutional affiliations.
516

Competing interests

518 The contact author has declared that none of the authors has any competing interests
519

Acknowledgments

521 The gratefully acknowledge support by NSF grants.
522

Financial support

524 This research has been supported by National Science Foundation (grant nos. OCE-1416837,
525 OCE-1737090, OCE 1736830, DISES 2108566, and RISE-2108566)

526

References

528

529 Anderson, T. W. (1994). Role of macroalgal structure in the distribution and abundance of a

530 temperate reef fish. *Marine ecology progress series. Oldendorf*, *113*(3), 279-290.

531   Beudin, A., Kalra, T. S., Ganju, N. K., & Warner, J. C. (2017). Development of a coupled wave-

532   flow-vegetation interaction model. *Computers & Geosciences*, *100*, 76-86.

533   Boch, C. A., Micheli, F., AlNajjar, M., Monismith, S. G., Beers, J. M., Bonilla, J. C., ... &

534   Woodson, C. B. (2018). Local oceanographic variability influences the performance of juvenile

535   abalone under climate change. *Scientific reports*, *8*(1), 1-12.

536   Britton, D., Cornwall, C. E., Revill, A. T., Hurd, C. L., & Johnson, C. R. (2016). Ocean

537   acidification reverses the positive effects of seawater pH fluctuations on growth and

538   photosynthesis of the habitat-forming kelp, Ecklonia radiata. *Scientific reports*, *6*(1), 26036.

539   Campbell, N. A., & Atchley, W. R. (1981). The geometry of canonical variate analysis. *Systematic*

540   *Biology*, *30*(3), 268-280.

541   Carter, G. S., Gregg, M. C., & Lien, R. C. (2005). Internal waves, solitary-like waves, and mixing

542   on the Monterey Bay shelf. *Continental Shelf Research*, *25*(12-13), 1499-1520.

543   Cavanaugh, K. C., Reed, D. C., Bell, T. W., Castorani, M. C., & Beas-Luna, R. (2019). Spatial

544   variability in the resistance and resilience of giant kelp in southern and Baja California to a

545   multiyear heatwave. *Frontiers in Marine Science*, *6*, 413.

546   Dayton, P. K. (1985). Ecology of kelp communities. *Annual review of ecology and*

547   *systematics*, *16*(1), 215-245.

548   Dayton, P. K., & Tegner, M. J. (1984). Catastrophic storms, El Niño, and patch stability in a

549   southern California kelp community. *Science*, *224*(4646), 283-285.

550   Deza, A. A., & Anderson, T. W. (2010). Habitat fragmentation, patch size, and the recruitment

551   and abundance of kelp forest fishes. *Marine Ecology Progress Series*, *416*, 229-240.

552   Duarte, C. M. (2017). Reviews and syntheses: Hidden forests, the role of vegetated coastal habitats

553   in the ocean carbon budget. *Biogeosciences*, *14*(2), 301-310.

554   Eger, A. M., Marzinelli, E. M., Beas-Luna, R., Blain, C. O., Blamey, L. K., Byrnes, J. E., ... &

555   Vergés, A. (2023). The value of ecosystem services in global marine kelp forests. *nature*

556   *communications*, *14*(1), 1894.

557   Fagundes, M., & Woodson, C. B. (2023). COAWST model files. Zenodo.

558   https://doi.org/10.5281/zenodo.10160564

559

560   Gaylord, B., Reed, D. C., Raimondi, P. T., Washburn, L., & McLean, S. R. (2002). A physically

561   based model of macroalgal spore dispersal in the wave and current-dominated

562   nearshore. *Ecology*, *83*(5), 1239-1251.

563   Gaylord, B., Rosman, J. H., Reed, D. C., Koseff, J. R., Fram, J., MacIntyre, S., ... & Mardian, B.

564   (2007). Spatial patterns of flow and their modification within and around a giant kelp

565   forest. *Limnology and Oceanograpy*, *52*(5), 1838-1852.

566   Haidvogel, D. B., Arango, H., Budgell, W. P., Cornuelle, B. D., Curchitser, E., Di Lorenzo, E., ...

567   & Wilkin, J. (2008). Ocean forecasting in terrain-following coordinates: Formulation and skill

568   assessment of the Regional Ocean Modeling System. *Journal of computational physics*, *227*(7),

569   3595-3624.

Kalra, T. S., Aretxabaleta, A., Seshadri, P., Ganju, N. K., & Beudin, A. (2017). Sensitivity analysis of a coupled hydrodynamic-vegetation model using the effectively subsampled quadratures method (ESQM v5. 2). *Geoscientific Model Development*, *10*(12), 4511-4523.

Ladah, L. B., Zertuche-González, J. A., & Hernández-Carmona, G. (1999). Giant kelp (Macrocystis pyrifera, Phaeophyceae) recruitment near its southern limit in Baja California after mass disappearance during ENSO 1997–1998. *Journal of Phycology*, *35*(6), 1106-1112.

Leary, P. R., Woodson, C. B., Squibb, M. E., Denny, M. W., Monismith, S. G., & Micheli, F. (2017). "Internal tide pools" prolong kelp forest hypoxic events. *Limnology and Oceanography*, *62*(6), 2864-2878.

Lentz, S. J., Kirincich, A., & Plueddemann, A. J. (2022). A note on the depth of sidelobe contamination in acoustic Doppler current profiles. *Journal of Atmospheric and Oceanic Technology*, *39*(1), 31-35.

Liu, Y., MacCready, P., Hickey, B. M., Dever, E. P., Kosro, P. M., & Banas, N. S. (2009). Evaluation of a coastal ocean circulation model for the Columbia River plume in summer 2004. *Journal of Geophysical Research: Oceans*, *114*(C2).

Low, N. H., Micheli, F., Aguilar, J. D., Arce, D. R., Boch, C. A., Bonilla, J. C., ... & Woodson, C. B. (2021). Variable coastal hypoxia exposure and drivers across the southern California Current. *Scientific reports*, *11*(1), 1-10.

Macreadie, P. I., Anton, A., Raven, J. A., Beaumont, N., Connolly, R. M., Friess, D. A., ... & Duarte, C. M. (2019). The future of Blue Carbon science. *Nature communications*, *10*(1), 3998.

590   Mancilla-Peraza, M., Palacios-Hernández, E., & López-Castillo, G. (1993). Hydrographic

591   Variability In Bahia Vizcaino, Baja California, Mexico. *Ciencias marinas*, *19*(3), 265-284.

592   Mcleod, E., Chmura, G. L., Bouillon, S., Salm, R., Björk, M., Duarte, C. M., ... & Silliman, B. R.

593   (2011). A blueprint for blue carbon: toward an improved understanding of the role of vegetated

594   coastal habitats in sequestering CO2. *Frontiers in Ecology and the Environment*, *9*(10), 552-560.

595   McPherson, M. L., Finger, D. J., Houskeeper, H. F., Bell, T. W., Carr, M. H., Rogers-Bennett, L.,

596   & Kudela, R. M. (2021). Large-scale shift in the structure of a kelp forest ecosystem co-occurs

597   with an epizootic and marine heatwave. *Communications biology*, *4*(1), 298.

598   Micheli, F., Saenz-Arroyo, A., Greenley, A., Vazquez, L., Espinoza Montes, J. A., Rossetto, M.,

599   & De Leo, G. A. (2012). Evidence that marine reserves enhance resilience to climatic

600   impacts. *PloS one*, *7*(7), e40832.

601   Monismith, S. G., Alnajjar, M. W., Woodson, C. B., Boch, C. A., Hernandez, A., Vazquez-Vera,

602   L., ... & Micheli, F. (2022a). Influence of kelp forest biomass on nearshore currents. *Journal of*

603   *Geophysical Research: Oceans*, *127*(7), e2021JC018333.

604   Monismith, S., Alnajjar, M., Daly, M., Valle-Levinson, A., Juarez, B., Fagundes, M., ... &

605   Woodson, C. B. (2022b). Kelp forest drag coefficients derived from tidal flow data. *Estuaries and*

606   *Coasts*, *45*(8), 2492-2503.

607   Murie, K. A., & Bourdeau, P. E. (2020). Fragmented kelp forest canopies retain their ability to

608   alter local seawater chemistry. *Scientific reports*, *10*(1), 11939.

609   Pakhomov, E., Kaehler, S., & McQuaid, C. (2002). Zooplankton community structure in the kelp

610   beds of the sub-Antarctic Prince Edward Archipelago: are they a refuge for larval stages?. *Polar*

611   *Biology*, *25*, 778-788.

612   Pawlowicz, R., Beardsley, B., & Lentz, S. (2002). Classical tidal harmonic analysis including error

613   estimates in MATLAB using T_TIDE. *Computers & geosciences*, *28*(8), 929-937.

614   Raffaelli, D., & Hawkins, S. J. (1996). *Intertidal ecology*. Springer Science & Business Media.

615   Reed, D., Rassweiler, A., & Arkema, K. (2009). Density derived estimates of standing crop and

616   net primary production in the giant kelp Macrocystis pyrifera. *Marine Biology*, *156*, 2077-2083.

617   Rosman, J. H., Koseff, J. R., Monismith, S. G., & Grover, J. (2007). A field investigation into the

618   effects of a kelp forest (Macrocystis pyrifera) on coastal hydrodynamics and transport. *Journal of*

619   *Geophysical Research: Oceans*, *112*(C2).

620   Rosman, J. H., Monismith, S. G., Denny, M. W., & Koseff, J. R. (2010). Currents and turbulence

621   within a kelp forest (Macrocystis pyrifera): Insights from a dynamically scaled laboratory

622   model. *Limnology and Oceanography*, *55*(3), 1145-1158.

623   Rosman, J. H., Denny, M. W., Zeller, R. B., Monismith, S. G., & Koseff, J. R. (2013). Interaction

624   of waves and currents with kelp forests (Macrocystis pyrifera): Insights from a dynamically scaled

625   laboratory model. *Limnology and Oceanography*, *58*(3), 790-802.

626 Russell, P., & Vennell, R. (2017). High-resolution observations of secondary circulation and

627 tidally synchronized upwelling around a coastal headland. *Journal of Geophysical Research:*

628 *Oceans*, *122*(2), 890-913.

629 Shchepetkin, A. F., & McWilliams, J. C. (2005). The regional oceanic modeling system (ROMS):

630 a split-explicit, free-surface, topography-following-coordinate oceanic model. *Ocean*

631 *modelling*, *9*(4), 347-404.

632 Schlenger, A. J., Beas-Luna, R., & Ambrose, R. F. (2021). Forecasting ocean acidification impacts

633 on kelp forest ecosystems. *PloS one*, *16*(4), e0236218.

634 Schiel, D. R., & Foster, M. S. (2015). *The biology and ecology of giant kelp forests*. Univ of

635 California Press.

636 Steneck, R. S., Graham, M. H., Bourque, B. J., Corbett, D., Erlandson, J. M., Estes, J. A., & Tegner,

637 M. J. (2002). Kelp forest ecosystems: biodiversity, stability, resilience and future. *Environmental*

638 *conservation*, *29*(4), 436-459.

639 Thomson, R. E., & Emery, W. J. (2014). *Data analysis methods in physical oceanography*.

640 Newnes.

641 Traiger, S. B., Cohn, B., Panos, D., Daly, M., Hirsh, H. K., Martone, M., ... & Nickols, K. J. (2022).

642 Limited biogeochemical modification of surface waters by kelp forest canopies: Influence of kelp

643 metabolism and site-specific hydrodynamics. *Limnology and Oceanography*, *67*(2), 392-403.

644   Trenberth, K. E. (1997). The definition of el nino. *Bulletin of the American Meteorological*

645   *Society*, *78*(12), 2771-2778.

646   Utter, B. D., & Denny, M. W. (1996). Wave-induced forces on the giant kelp Macrocystis pyrifera

647   (Agardh): field test of a computational model. *Journal of experimental Biology*, *199*(12), 2645-

648   2654.

649   Valle-Levinson, A., Daly, M. A., Juarez, B., Tenorio-Fernandez, L., Fagundes, M., Woodson, C.

650   B., & Monismith, S. G. (2022). Influence of kelp forests on flow around headlands. *Science of the*

651   *Total Environment*, *825*, 153952.

652   Warner, J. C., Geyer, W. R., & Lerczak, J. A. (2005). Numerical modeling of an estuary: A

653   comprehensive skill assessment. *Journal of Geophysical Research: Oceans*, *110*(C5).

654   Warner, J. C., Sherwood, C. R., Signell, R. P., Harris, C. K., & Arango, H. G. (2008). Development

655   of a three-dimensional, regional, coupled wave, current, and sediment-transport model. *Computers*

656   *& geosciences*, *34*(10), 1284-1306.

657   Walter, R. K., Woodson, C. B., Arthur, R. S., Fringer, O. B., & Monismith, S. G. (2012). Nearshore

658   internal bores and turbulent mixing in southern Monterey Bay. *Journal of Geophysical Research:*

659   *Oceans*, *117*(C7).

660   Wernberg, T., Krumhansl, K., Filbee-Dexter, K., & Pedersen, M. F. (2019). Status and trends for

661   the world's kelp forests. In *World seas: An environmental evaluation* (pp. 57-78). Academic Press

662   Willmott, C. J. (1981). On the validation of models. *Physical geography*, *2*(2), 184-194.

663 Woodson, C. B. (2018). The fate and impact of internal waves in nearshore ecosystems. *Annual*

664 *review of marine science*, *10*, 421-441.

665 Wu, Y., Hannah, C. G., O'Flaherty-Sproul, M., & Thupaki, P. (2017). Representing kelp forests in

666 a tidal circulation model. *Journal of Marine Systems*, *169*, 73-86.

667

668